ADVANCES IN ATMOSPHERIC SCIENCES, VOL. 34, MAY 2017, 663–678

• **Original Paper** •

Global Land Surface Climate Analysis Based on the Calculation of a Modified Bowen Ratio

Bo HAN*[1], Shihua LÜ[2,3], Ruiqing LI[4], Xin WANG[1], Lin ZHAO[1], Cailing ZHAO[5], Danyun WANG[1], and Xianhong MENG[1]

[1]*Key Laboratory of Land Surface Process and Climate Change in Cold and Arid Regions, Cold and Arid Regions Environmental and Engineering Research Institute, Chinese Academy of Sciences, Lanzhou* 730000*, China*

[2]*College of Atmospheric Sciences, Chengdu University of Information Technology Plateau Atmosphere and Environment Key Laboratory of Sichuan Province, Chengdu* 610225*, China*

[3]*Collaborative Innovation Center on Forecast and Evaluation of Meteorological Disasters, Nanjing University of Information Science and Technology, Nanjing* 210044*, China*

[4]*Inner Mongolia Autonomous Regional Meteorological Observatory, Hohhot* 010051*, China*

[5]*Institute of Arid Meteorology, China Meteorological Administration, Lanzhou* 730020*, China*

(Received 3 August 2016; revised 27 October 2016; accepted 11 November 2016)

ABSTRACT

A modified Bowen ratio (BRm), the sign of which is determined by the direction of the surface sensible heat flux, was used to represent the major divisions in climate across the globe, and the usefulness of this approach was evaluated. Five reanalysis datasets and the results of an offline land surface model were investigated. We divided the global continents into five major BRm zones using the climatological means of the sensible and latent heat fluxes during the period 1980–2010: extremely cold, extremely wet, semi-wet, semi-arid and extremely arid. These zones had BRm ranges of $(-\infty, 0)$, $(0, 0.5)$, $(0.5, 2)$, $(2, 10)$ and $(10, +\infty)$, respectively. The climatological mean distribution of the Bowen ratio zones corresponded well with the Köppen-like climate classification, and it reflected well the seasonal variation for each subdivision of climate classification. The features of climate change over the mean climatological BRm zones were also investigated. In addition to giving a map-like classification of climate, the BRm also reflects temporal variations in different climatic zones based on land surface processes. An investigation of the coverage of the BRm zones showed that the extremely wet and extremely arid regions expanded, whereas a reduction in area was seen for the semi-wet and semi-arid regions in boreal spring during the period 1980–2010. This indicates that the arid regions may have become drier and the wet regions wetter over this period of time.

Key words: climate classification, surface turbulent heat flux, climate change

Citation: Han, B., and Coauthors, 2017: Global land surface climate analysis based on the calculation of a modified Bowen ratio. *Adv. Atmos. Sci.*, **34**(5), 663–678, doi: 10.1007/s00376-016-6175-y.

1. Introduction

The patterns observed in Earth's climate over the surface of the continents are related to the distribution of vegetation and are thus spatially heterogeneous. An approach is needed to classify the continental climate based on variations in the landscape. The first widely accepted classification of climate was proposed by Koöppen (1931) and was based on the idea that the native vegetation of a region is the best expression of its climate. This initial classification was modified by Trewartha and coworkers (Trewartha and Sale, 1968; Trewartha and Horn, 1980) and, based on these earlier studies, a world map of climate classification was proposed (Kottek et al., 2006; Peel et al., 2007).

The method used for the Koöppen-like climate classification (KCC) is based on the monthly surface air temperature (SAT) and the rate of precipitation. As the latter parameter largely determines the local humidity near Earth's surface, KCC focuses on the natural underlying hydrothermal status of landscapes. Reliable, long-term site observation records are available for both SAT and precipitation (Jones et al., 1999; Chen et al., 2002), which means that KCC is both objective and simple to use (Feng et al., 2012; Tang and Hossain, 2012; Gallardo et al., 2013; Elguindi et al., 2014). The KCC map corresponds well to maps of ecological regions

* Corresponding author: Bo HAN
Email: hanbo@lzb.ac.cn

(Warry and Hanau, 1993; Olson et al., 2001; Menon et al., 2010; Pearch, 2011), although these are based on the distribution of species and communities. The functional types of plants represent the close connection between the land surface cover and environmental conditions (Golluscio and Sala, 1993; Smith et al., 1993; Condit et al., 1996; Woodward and Cramer, 1996; Rusch et al., 2003; Navarro et al., 2006; Ustin and Gamon, 2010).

KCC divides the global continental climate into five or six major divisions, including the equatorial zone, the arid zone, the warm temperate zone, the snow zone, and the polar zone, all of which include several subdivisions (Trewartha and Horn, 1980; Kottek et al., 2006; Peel et al., 2007). On the global scale, the major divisions of climate classification systems seem to be more useful in climate analysis than their subdivisions. For example, arid and semi-arid (SA) regions are usually considered together in analyses of climate change (Ragab and Prudhomme, 2002; Holmgren et al., 2006; Poulter et al., 2014), regardless of the fact that they usually correspond to deserts and temperate grasslands, respectively. Other indices have also been used to show the major divisions in climate; for example, the United Nations Environment Programme has used several aridity indices based on the balance of water or energy fluxes on the land surface to produce a map of "dryness" (Budyko, 1961; Middleton and Thomas, 1997). Indices derived from remotely sensed data, such as the normalized difference vegetation index, can also tell the differences in land surface from the viewpoint of vegetation cover (Defries and Townshend, 1994; Walker et al., 2003; Wang et al., 2005; Zhang et al., 2014; Sun et al., 2015).

The turbulent energy fluxes within the surface boundary layer reflect the hydrothermal characteristics near the land surface. The surface sensible heat has a large positive (i.e., upward) value over hot regions, such as deserts, and small or even negative (i.e., downward) values over cold regions, such as Greenland. By contrast, the humidity status of soil largely modifies the latent heat flux (or evapotranspiration rate), and both of them are largely determined by local precipitation. Besides, in some regions with little precipitation, like an oasis, the soil can be humid and the evaporation is strong due to other kinds of water supplements, like inland rivers or artificial irrigation (Paltineanu et al., 2011). Changes in the underlying surface are more rapidly reflected in changes in the turbulent heat fluxes than in the local SAT and rate of precipitation, which are mainly modified by large-scale atmospheric circulation.

The Bowen ratio (BR) was originally defined as the ratio between the sensible heat flux and the latent heat flux (Bowen, 1926; Lewis, 1995):

$$\mathrm{BR} = \frac{H_\mathrm{S}}{lE}\,, \tag{1}$$

where H_S is the sensible surface heat flux (upwardly positive), E is the evapotranspiration rate (upwardly positive), and l is the latent heat of vaporization of water. The BR partly reflects the intensity of evapotranspiration (or water use) or the humidity over different types of underlying surface over a long period of time (Pitacco et al., 1992; den Hartog et al., 1994; Todd et al., 2000; Inman-Bamber and McGlinchey, 2003). An arid, warm region generally has a large BR, whereas a humid, cool region usually has a small BR. As the BR partly reflects the hydrothermal features in the surface boundary layer, we used it to describe the global continental climate.

2. Data and methods

2.1. *Datasets*

Unlike the SAT or rate of precipitation, neither the sensible nor the latent heat flux could be precisely monitored by field observations until the development of eddy covariance techniques (Dabberdt et al., 1993; den Hartog et al., 1994; Baldocchi et al., 1996, 2001; Toda et al., 2002; Wilson et al., 2002; Baldocchi, 2003; Krishnan et al., 2012). There are only a few tens of observation sites worldwide that have recorded the turbulent heat flux for more than 10 years, and not all of these sites share their data. The observed surface turbulent heat fluxes still contain uncertainties as a result of the design of equipment and the flux source area (footprint) (Fisher et al., 2008), and are therefore not suitable for the determination of global land–air interactions. Global surface energy heat fluxes are, however, available in many datasets based on model products, such as reanalysis data or data from IPCC AR5 (Taylor et al., 2012). Although these model-based products have limitations, they are generally able to give a qualitative description of the surface climate over different underlying surfaces. This encouraged us to investigate features of the global land surface by comparing the land surface heat fluxes from different kinds of datasets.

Reanalysis datasets have been used to build sensible and latent heat fluxes over the oceans (Yu et al., 2008). The energy fluxes at Earth's surface from reanalysis datasets are produced directly by numerical land surface models (usually based on bulk formulas) without assimilation with observations. The uncertainty within the numerical models will lower the reliability of these data. Nevertheless, when the temperature, humidity and parameters (like roughness) within the surface layer can be determined correctly, reanalysis can produce a reasonable spatial distribution pattern for global sensible and latent heat fluxes.

Five reanalysis datasets were chosen: (1) ERA-Interim (ERA-I) (Dee et al., 2011); (2) NCEP–NCAR (NCEP-R1) (Kalnay et al., 1996); (3) NCEP–DOE AMIP-II (NCEP-R2) (Kanamitsu et al., 2002); (4) JRA-55 (Kobayashi et al., 2015); and (5) 20th century reanalysis, version 2 (20thC) (Compo et al., 2011). Monthly means for four variables—SAT, precipitation rate, sensible and latent heat fluxes—were used in this study. The ensemble mean (EM) of the reanalysis data can be expected to minimize the uncertainty, so this was our primary focus. A product from the Global Land Data Assimilation System (GLDAS) (Rodell et al., 2004) was also used. GLDAS has been developed jointly by scientists at NASA's GSFC (Goddard Space Flight Center) and the Na-

tional Oceanic and Atmospheric Administration's NCEP. It makes use of the latest generation of ground- and space-based observation systems, to force and evaluate different kinds of land surface model. In the second version of GLDAS used in this study, only the data from the Noah land surface model has been published so far. A general description of all datasets used is given in Table 1, noting the difference in land-surface models. For convenience, we re-gridded all the datasets onto a $1^\circ \times 1^\circ$ grid.

2.2. *Modified Bowen ratio*

A negative latent heat flux can exist when the condensation of water vapor is greater than evapotranspiration near the land surface (Bintanja, 2000; Jacobs et al., 2008). Therefore, a negative BR may correspond to either a negative sensible heat flux or a negative latent heat flux. The sensible and latent heat fluxes over the Arctic or Antarctic regions can both be negative at the same time, leading to a positive BR close to that measured in temperate zones. To avoid the possibility of a cold region showing a similar BR to a temperate region, the modified BR is defined as

$$\mathrm{BRm} = \left|\frac{H_\mathrm{S}}{lE}\right| \times \mathrm{sgn}(H_\mathrm{S}) \,, \tag{2}$$

where the function $\mathrm{sgn}(x)$ gives the sign of the variable x. Using this definition, the BRm will always be negative when the local sensible heat flux is negative (i.e. downwards) regardless of the sign (or direction) of the latent heat flux. Thus, the BRm can distinguish a cold region from a warm region using the direction of the sensible heat flux.

The absolute value of the local BRm can be extremely large if the value of lE is close to zero. To avoid the effect of a large BRm on the average calculation, the average BRm ($\langle \mathrm{BRm} \rangle$), regardless of the spatial or temporal scale or for an EM of several datasets, are derived not from the ensemble of BRms (for all grids or time steps) but from the corresponding averages of the surface heat fluxes:

$$\langle \mathrm{BRm} \rangle = \left|\frac{\langle H_\mathrm{S} \rangle}{\langle lE \rangle}\right| \times \mathrm{sgn}(\langle H_\mathrm{S} \rangle) \,. \tag{3}$$

The Antarctic continent was not included in this study as a result of the large discrepancy in the surface atmospheric variables in reanalysis (Nicolas and Bromwich, 2014). This is due to the low number of long-term observations in this region (Turner et al., 2005).

3. Results

Figure 1 shows the climatological mean BRm determined from the EM of the reanalysis of the datasets. The distribution patterns of the climatological mean BRm (1980–2010) determined from all the datasets were similar and the correlation coefficients of the spatial patterns using the EM BRm were all greater than 0.6. These results encouraged us to use the BRm to represent different climatic zones.

3.1. *Globally averaged Bowen ratios*

The globally averaged BRm over the continent north of 60°S reflects the general hydrothermal status of the global land surface (Fig. 2). Most of the datasets tended to give a positive climatological mean BRm, both in each season and annually, except for the NCEP-R2 dataset in winter (December, January and February; DJF). The climatological mean values of BRm for all seasons and the annual mean from all reanalyses were less than 1, indicating that the average latent heat flux was greater than the sensible heat flux.

The globally averaged values of BRm decreased linearly in all seasons during the period 1980–2010. There were some exceptions to this, including the JRA-55 dataset in spring (March, April, May; MAM), the 20thC dataset in summer (June, July, August; JJA) and the NCEP-R1 dataset in autumn (September, October, November; SON). This negative trend in the values of BRm means that the available energy is partitioned more towards the latent heat flux. This is identical to the increase in global vegetation density (Bounoua et al., 2000) that occurs in SA regions (Fensholt et al., 2012) as a result of surface warming, especially over the mid- to high-latitude zones in the Northern Hemisphere (Zhou et al., 2003).

The climatological mean globally averaged BRm given by GLDAS was much larger than those from other reanalyses. The sensible heat flux in GLDAS was greater and the latent heat flux was smaller than those in reanalysis datasets. For example, in JJA, the climatological mean of globally averaged sensible heat flux over land was 70.3 W m^{-2} in GLDAS, while the maximum of the reanalyses was given by 20thC, being 54.7 W m^{-2}. As for the mean latent heat flux in JJA, the result given by GLDAS was only 44.5 W m^{-2}, and the smallest result from the reanalyses was given by JRA-55, being 55.2 W m^{-2}. One potential reason for the differences is that GLDAS does not consider the feedback from land–surface processes to atmospheric circulation. However, whether the results from reanalysis are better than GLDAS is

Table 1. Details regarding the datasets used in this study.

Name	Duration	Resolution (Lat × lon)	Land-surface model
ERA-I	1979 to present	$1.5^\circ \times 1.5^\circ$	TESSEL (Viterbo and Beljaars, 1995)
20thC	1871 to present	$1^\circ \times 1^\circ$	Noah land surface model (Ek et al., 2003)
NCEP-R1	1948 to present	$1^\circ \times \sim 1.875^\circ$	OSU model (Pan and Mahrt, 1987)
NCEP-R2	1979 to present	$1^\circ \times \sim 1.875^\circ$	OSU model (Pan and Mahrt, 1987)
JRA55	1958 to present	$1.25^\circ \times 1.25^\circ$	Simple Biosphere model (Sellers et al., 1986)
GLDAS (V2)	1948 to 2010	$1^\circ \times 1^\circ$	Noah land surface model (Ek et al., 2003)

not easy to ascertain.

The temporal correlation coefficients of the annual globally averaged values of BRm between each dataset and the EM of the reanalyses were significant (Table 2); the only exception was from the ERA-I dataset in JJA. The correlation coefficients of the values of the BRm between GLDAS and the EM were also significant, except in JJA and SON. Identical interannual variations in the value of BRm across most datasets can be attributed to the southern oscillation index, which has the largest impact on the pattern of global precip-

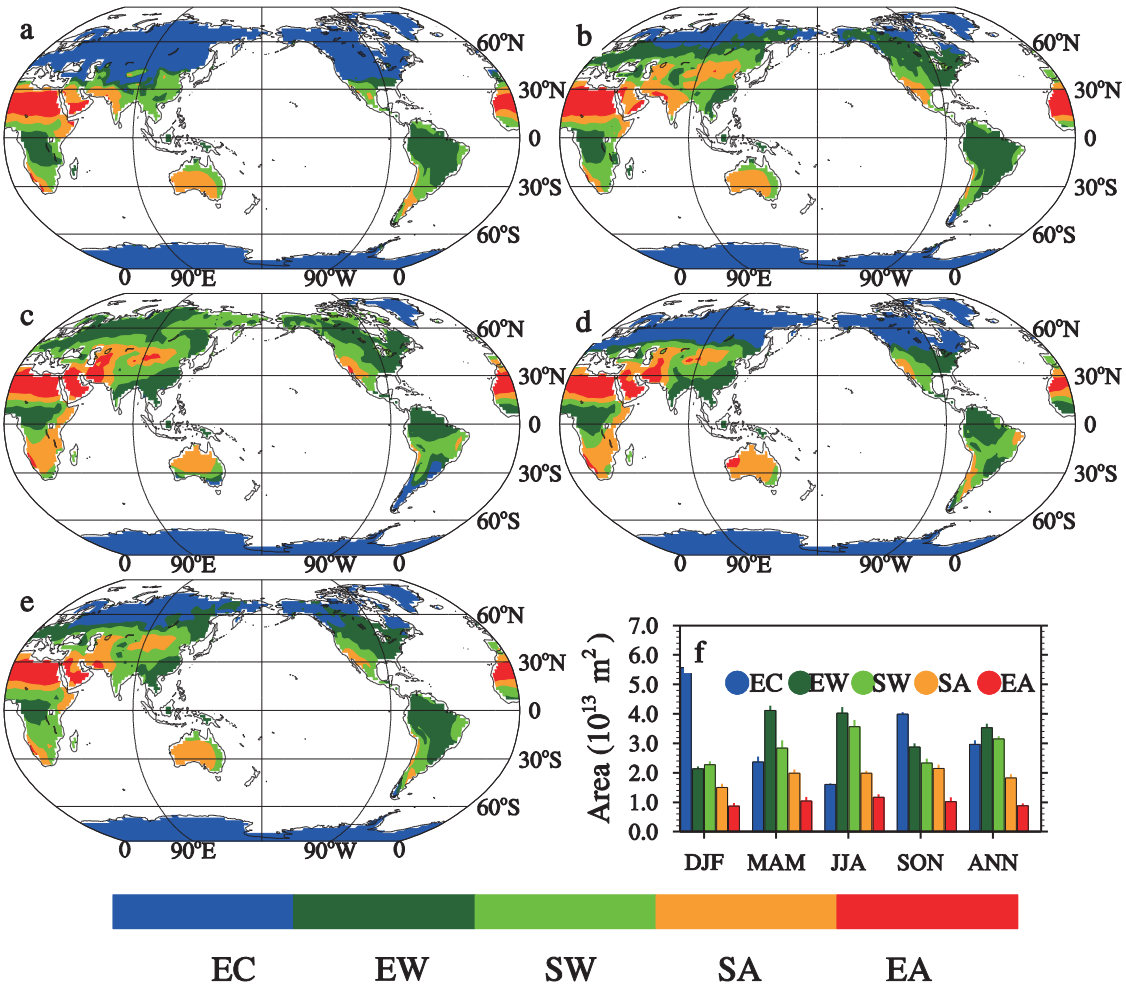

Fig. 1. Patterns of mean climatological BRm in (a) DJF, (b) MAM, (c) JJA, (d) SON and (e) annual means (ANN) for the period 1980–2010. Results are derived from the EM of the five reanalysis datasets. Contour intervals are 4, 0.1, 0.3, 2 and 4 for the BRm ranges of the five zones, respectively: (−∞ to 0; EC, blue); (0–0.5; EW, dark green); (0.5–2.0; SW, green); (2.0–10; SA, yellow); and (10 to +∞; EA, orange). The total areas of the five BRm zones (columns; units: 1013 m^2) and the standard deviations (error bars; units: 10^{13} m^2) are shown in (f).

Table 2. Correlation coefficients for the annual global mean Bowen ratios during 1980–2010 between the datasets used in this study and the ensemble mean of the reanalyses.

	Dataset					
	20thC	NCEP-R1	NCEP-R2	ERA-I	JRA55	GLDAS
DJF	0.83	0.79	0.87	0.87	0.56	0.46
MAM	0.69	0.73	0.68	0.64	0.54	0.36
JJA	0.47	0.63	0.71	0.10*	0.57	0.14*
SON	0.72	0.59	0.50	0.48	0.47	0.21*
Annual mean	0.53	0.66	0.62	0.39	0.67	0.34

Note: *Not statistically significant ($P > 0.05$).

DJF, December, January, February; MAM, March, April, May; JJA, June, July, August; SON, September, October, November.

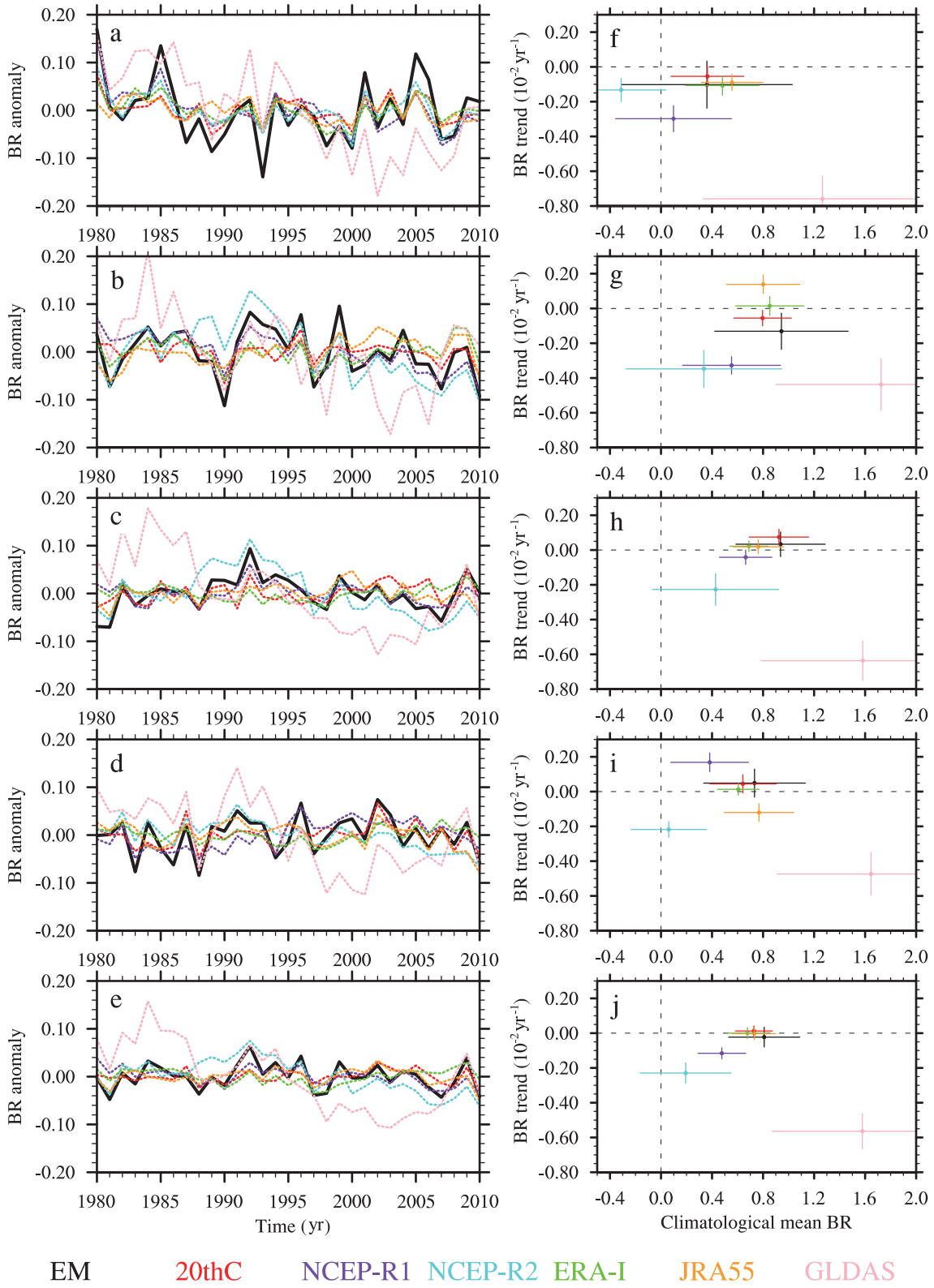

Fig. 2. Spatially averaged BRm anomalies north of 60°S for (a) DJF, (b) MAM, (c) JJA, (d) SON and (e) annual means from 1980 to 2010. The climatological means and trends (units: 10^2 yr^{-1}) in 1980–2010 are shown in the right-hand column (f–j); the horizontal error bars are the standard deviation ×100 for convenience of display and the vertical error bars are the standard error (units: 10^2 yr^{-1}) of the BRm trends.

itation on an interannual timescale (Bradley et al., 1987; Dai and Wigley, 2000). There was a weak negative correlation between the southern oscillation index and the continental averaged BR. The correlation coefficients in DJF ranged from −0.1 (20thC) to −0.38 (GLDAS). However, the sensitivity of the BRm to the local precipitation depends on the base cli-

mate. For example, the responses to the dry season in intact forests and pastures near the Amazon region have been reported to be the opposite of each other (Huete et al., 2006).

3.2. *Patterns in the climatological mean Bowen ratio*

We investigated whether the patterns in the BRm captured the main features of KCC (Kottek et al., 2006; Peel et al., 2007). With reference to KCC, we suggest that there are five major BRm zones: BRm < 0 in extremely cold (EC) regions, which means the sensible heat flux should be negative; $0 \leqslant$ BRm < 0.5 in extremely wet (EW) regions—a much greater latent heat flux than sensible one; BRm > 10 in extremely arid (EA) regions—opposite situation as in EW; and regions with BRm ranging from 0.5 to 2 and from 2 to 10, representing semi-wet (SW) and SA regions, respectively. These threshold values were empirically chosen in this study, with consideration that a wet (arid) region should feature a greater (smaller) latent heat flux than sensible one near the land surface. These values can to some extent be verified in other research. The area of each climatological mean BRm zone in DJF and JJA was similar (Table 3), except that the NCEP-R2 dataset produced a much smaller area for EA regions. The SA region given by GLDAS was much larger than that generated from the reanalyses.

There were some similarities in the major divisions between the KCC and the climatological annual mean BRm zones (Fig. 1e). For example, the SA and EA regions were generally contained within the arid region in the KCC; the EC regions covered the main area of the snow and polar regions in the KCC; and the sum of the tropical and warm temperate regions in the KCC generally corresponded to the EW and SW regions.

Some regions showed different BRm zones in different seasons. Based on the seasonal variations in the BRm, the major BRm zones could be further divided into several subdivisions. By comparing the climatological BRm for the annual mean with that for the seasonal means, four scenarios were observed: (1) the BRm zones for all seasons were the same as that for the annual mean (colored green in Fig. 3); (2) the mean BRm in any season (usually a wet or cold season) was less than the minimum, and that for all seasons was smaller than the maximum of the BRm range for the annual mean (colored blue in Fig. 3); (3) the mean BRm in any season (usually a dry or hot season) was greater than the maximum, and that for all seasons was greater than the minimum of the BRm range for the annual mean (colored red in Fig. 3); and (4) the mean BRm in any season was smaller than the minimum, and the mean BRm in another season was greater than the maximum of the range for the annual mean (colored purple in Fig. 3). Based on these four scenarios, the major BRm zones were divided into four subdivisions. For convenience, each subdivision was named as the BRm zone plus an index number. For example, an EC region that met the conditions of scenario 1 was referred to as EC1. The EA regions were only divided into two subdivisions (EA1 and EA2) and the EC regions into EC1 and EC3; the rest of the BRm zones were divided into all four subdivisions.

3.2.1. *Extremely cold regions*

The EC regions corresponded to snow-covered or polar climatic zones in the KCC. In addition to Antarctica, the EC region covered a large area north of 40°N in the northern hemisphere in DJF, including the main region of permafrost. By contrast, in JJA the EC region was located only in Greenland. Figure 3a shows that the polar climate corresponded well to EC1, covering Greenland and the Antarctic continent, whereas the snow climate was expressed well by EC3, which covered large areas of Russia and Canada.

The Tibetan Plateau was classified as polar tundra by the KCC, which means that the SAT and precipitation were similar to those recorded in Siberia or Canada. However, only the northern edge of Tibet had a negative BRm in DJF (Fig. 1a). During most of the year, Tibet had a BRm value between 1 and 4, similar to an SW or SA region. Therefore, based on the results from the reanalysis, the land–air interaction over the Tibetan Plateau may have different characteristics from those over the polar tundra. Other highland regions in low or middle latitudinal zones, such as the Rocky Mountains in North America, also exhibited similar BRm characteristics to the Tibetan Plateau.

3.2.2. *Extremely wet regions*

The main equatorial climate zones in the KCC covered the main rainforest regions, including the Congo Basin,

Table 3. Mean area (10^{13} m^2) of climatological modified Bowen ratio zones in December, January, February (DJF) and June, July, August (JJA).

	DJF					JJA				
Dataset	EC	EW	SW	SA	EA	EC	EW	SW	SA	EA
20thC	5.9	2.9	2.7	2.0	1.3	2.0	4.2	4.3	2.2	2.0
NCEP-R1	6.3	3.2	1.9	1.4	1.8	2.7	5.4	2.5	1.7	2.4
NCEP-R2	7.8	3.2	2.3	1.3	0.1	3.7	5.4	3.4	1.8	0.4
ERA-I	5.1	3.7	3.3	1.4	1.1	1.8	5.6	4.6	1.4	1.3
JRA55	5.4	2.4	2.9	1.1	0.8	1.6	3.3	5.1	1.6	1.0
EM	5.6	2.1	2.3	1.5	0.9	1.6	4.0	3.6	2.0	1.2
GLDAS	5.1	1.8	3.5	2.7	1.7	1.7	2.5	4.9	3.7	1.8

Note: EC, extremely cold; EW, extremely wet; SW, semi-wet; SA, semi-arid; EA, extremely arid.

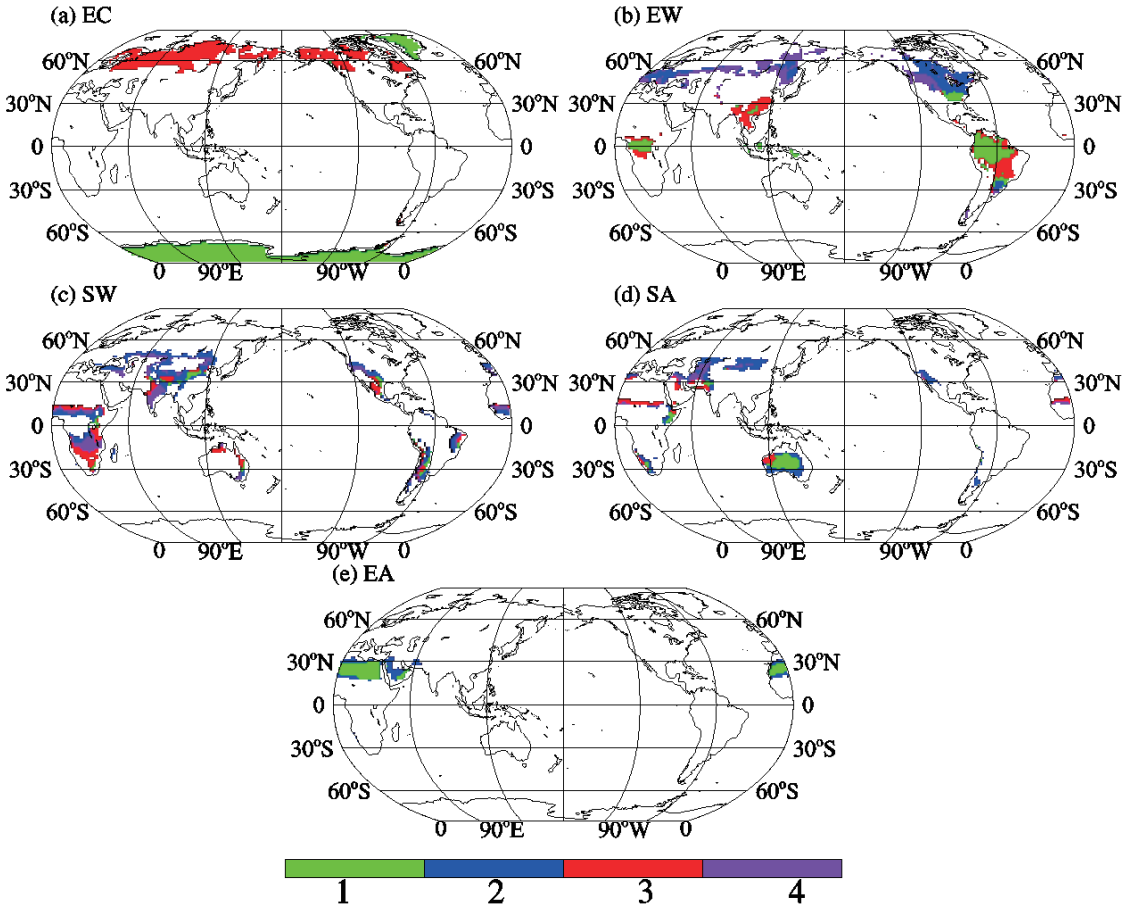

Fig. 3. Subdivisions for (a) EC, (b) EW, (c) SW, (d) SA and (e) EA regions derived from the EM of the reanalysis datasets. The subdivisions are summarized by comparing the climatological BRm for the seasonal mean with that for the annual mean. Four scenarios are listed: (1) the types of BRm zones for all seasons are the same as the annual mean (green); (2) the mean BRm in any season is smaller than the minimum, and that in all seasons is smaller than the maximum of the BRm range for the annual mean (blue); (3) the mean BRm in a season is greater than the maximum, and that in all seasons is greater than the minimum of the BRm range for the annual mean (red); and (4) the mean BRm in any season is smaller than the minimum, and that in another season is greater than the maximum of the range for the annual mean (purple).

Malaysia, New Guinea and the Amazon Basin. They were well expressed by EW1, indicating only a small seasonal variation in the BRm. The southeastern USA was also covered by EW1. The main EW3 regions were adjacent to the EW1 regions, such as tropical Africa, China and Brazil. The large seasonal variation in the BRm was a result of the concentrated precipitation during the summer monsoon (Zhou and Lau, 1998; Gan et al., 2004).

The EW2 and EW4 regions covered large areas north of 30°N. In the EW2 regions, such as Northeast America and Europe, the summer EW region became an EC region in winter. This was due to the presence of wetlands in the form of fens and bogs (Aselmann and Crutzen, 1989), in addition to the forested area. These wetlands can sustain a large latent heat flux in JJA, but are usually frozen or snow-covered in the cold season. In the EW4 regions, such as the western central part of America and southern Siberia, the lack of precipitation in the dry season lowered the surface evaporation rate to that of an SW region.

3.2.3. *Semi-wet regions*

The seasonal variation in the BRm showed the most distinctive spatial difference on a global scale for the SW regions. As these regions were the transition zone from wet to arid regions, the seasonal variation in BRm in SW regions was determined by the distance from the nearby EW zones. An SW region close to an EW region was mostly of type SW2, whereas one that was close to an SA region was mostly SW3.

The strong seasonal variation in BRm in SW4 can be attributed to monsoon precipitation. Two SW4 regions corresponded well to the main monsoon regions. The first region was mainland India, which corresponded to the South Asia summer monsoon area, and the second region was located near 10°N in Africa, corresponding to the West Africa monsoon area. The rest of the SW4 regions were located in the

temperate steppe region of central Asia and the savanna region (10°–20°S) of Africa.

3.2.4. *Semi-arid regions*

The SA region between 30°N and 30°S was defined as hot arid desert or hot arid steppe in the KCC. It generally corresponded to an underlying surface of desert, such as mainland Australia. The seasonal variation in the value of BRm in central Australia was small, and this region was therefore defined as SA1. The rest of the SA regions at low latitudes were generally SA3, and became EA in the dry season.

By contrast, the SA regions outside the tropical regions were defined as cold arid desert or cold arid steppe in the KCC. The cold arid desert regions were expressed as SA4 in our classification, and the cold arid steppe regions corresponded to SA2. In addition to the temperature difference between summer and winter, the high precipitation in the cold season, as seen in Northwest China, probably contributed to the large seasonal variation in the value of BRm (Small et al., 1999).

In the 20°–30°S belt, the KCC suggested the hot arid desert or hot arid steppe to be dominant in Australia, whereas the cold arid desert or cold arid steppe was represented in Africa. The difference between these two regions was also obvious in the BRm. The former regions were classified as SW3 and SW4, whereas the latter were classified as SA1, SA2 and SA3.

3.2.5. *Extremely arid regions*

The EA regions covered the Sahara desert and Arabian Peninsula (Fig. 3e). These two regions were classified as hot arid desert in the KCC. The main regions in the Sahara desert were classified as EA1. The EA2 regions were located on the northern edge and in the western part of the Arabian Peninsula, corresponding to a Mediterranean climate. As there were also SA3 regions in the Arabian Peninsula (Fig. 3d), the spatial differences in the land surface processes were notable in this region, although the whole Arabian Peninsula was defined as hot arid desert in the KCC.

Using BRm can therefore capture the broad global distribution of climatic zones. Compared with the KCC, the BRm zones are classified based on land surface processes, so it can differentiate some regions based on land–air interactions, despite the fact that they have the same type of climate in the KCC.

3.2.6. *Seasonal variation of precipitation within BR zones*

The seasonal precipitation rates within global BR zones are given in Fig. 4. Here, the BR zones in each seasons are defined the same as the climatological annual mean of BRm (as in Fig. 1e), and only the climatological mean precipitation has been considered. Most datasets agreed that the seasonal variation of precipitation in EC and EW are similar, showing maximum precipitation in JJA and minimum in DJF. Meanwhile, in SW regions, the greatest precipitation rate was still in JJA, but in the rest of the seasons the differences in precipitation were small. The EM of the reanalyses gave the smallest precipitation rate for the SW regions in MAM, but the discrepancy among datasets was large. In SA regions, the strongest precipitation took place in DJF, and the precipitation rate in SON was the smallest in most datasets. The seasonal difference in precipitation was smallest in EA regions. The intraseasonal variation of precipitation can be attributed to several large-scale modification processes of atmospheric circulation, such as the onset of the monsoon system or polar vortex.

3.3. *Climate change in climatological Bowen ratio zones*

Because all the datasets used in this study also contain the fields of SAT and precipitation, the characteristics of climate change can be discussed in terms of the major divisions in the climatological mean BRm. The mechanism for the different responses of the SAT and the rate of precipitation in these BRm zones was beyond the scope of this study.

3.3.1. *Surface warming*

The change in SAT differed in the climatological mean BRm zones during the period 1980–2010 (Fig. 5). The rate of warming was much greater in the EC regions than in the other BRm zones in MAM and SON, at 4.4 and 5.8 ($\times 10^{-2}$ K yr^{-1}) from the EM, respectively. In DJF and JJA, however, the EA region showed the greatest warming rate of 5.1 and 4.0 ($\times 10^{-2}$ K yr^{-1}) from the EM, respectively. Although most projections of future climate change indicate that the high latitude regions of the Northern Hemisphere, where the main EC region is located, will experience the greatest warming worldwide (Giorgi et al., 2001), there was no such trend in the results for DJF, JJA and the annual mean in past decades from the reanalyses considered here. The weaker warming in the EC region in DJF was related to the increased precipitation (snowfall) over part of the EC region, such as in central Asia (not shown). The warming rates for the SA, SW and EW regions were modest in most seasons.

Huang et al. (2012) considered the regions with a mean precipitation of 200–600 mm yr^{-1} to be SA. They concluded that the warming rate is much greater over SA regions than over arid or humid regions in the cold season. However, by that measure, the SA category contains a large area of the EC region in high latitudinal zones such as Siberia. In addition, both observations and simulation analyses tend to suggest that SA regions, which are usually located in the mid- to low-latitude belt, do not have a much stronger warming rate than high latitudes in boreal winter (Wallace et al., 2012). In this study, the warming rate over SA regions during the period 1980–2010 was modest compared with the EA and EC regions.

3.3.2. *Precipitation trends*

There were larger uncertainties in the precipitation trends over continents among the datasets than in the SATs (Fig. 6a). A decrease in the annual mean precipitation was seen in four of six of the reanalysis datasets. There was no certain change in the annual mean precipitation rate in the other BRm zones.

Most datasets tended to show an increase in precipitation

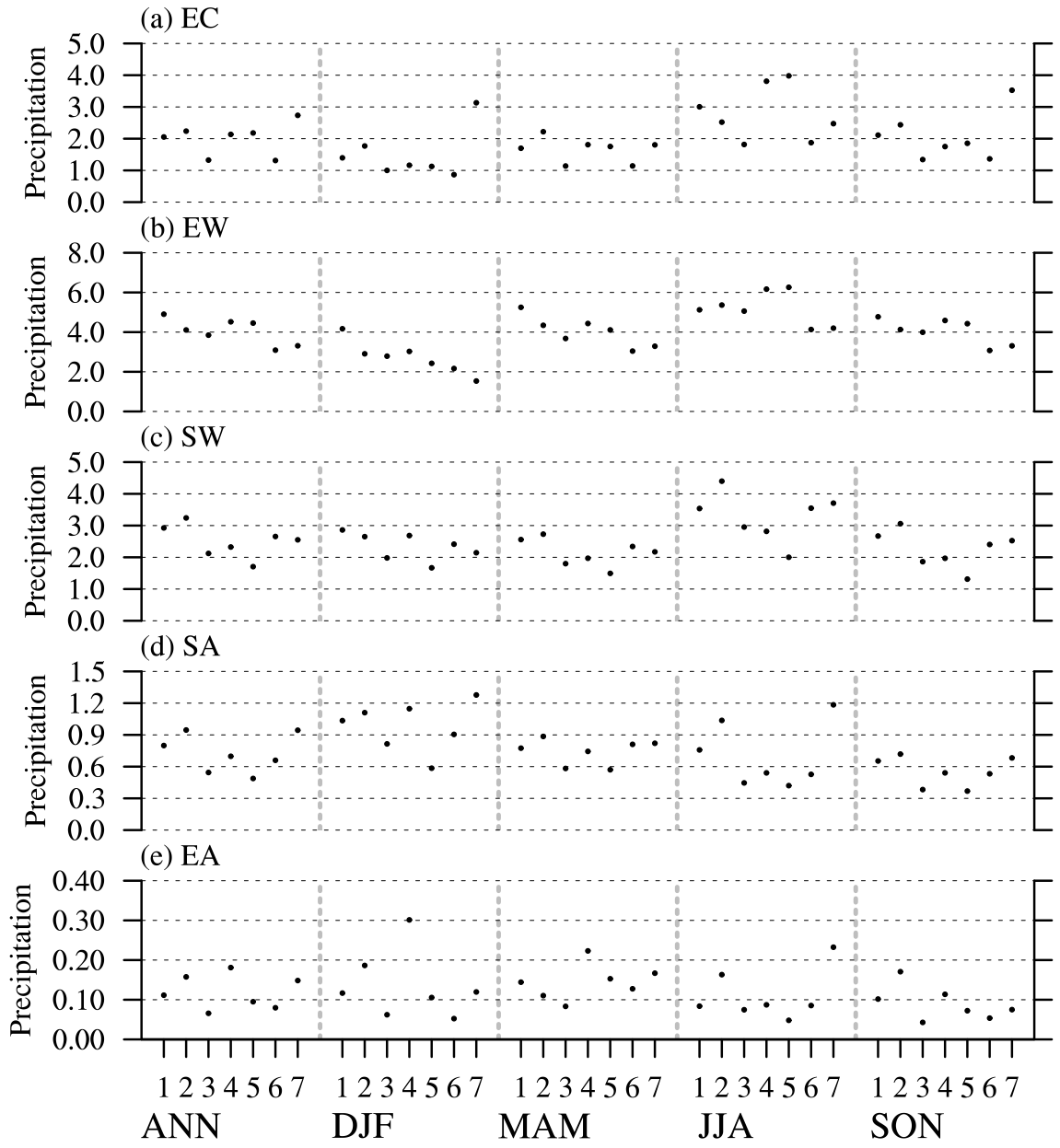

Fig. 4. Climatological means of regional averaged precipitation (units: 10^{-5} kg m^{-2} s^{-1}) within BR zones in different seasons during the time period 1980–2010. The BR zones are defined based on the pattern of climatological annual means of BRm. The number on the abscissa represents different datasets: 1, ensemble mean of the reanalysis data; 2, 20thC; 3, ERA-I; 4, NCEP-R1; 5, NCEP-R2; 6, JRA55; and 7, GLDAS dataset.

in DJF in the EW, SW and SA regions. This increase in precipitation generally caused a cooling and moistening process, reducing the BRm on a global scale (Fig. 2a). This increased precipitation was associated with cooling of the land surface, e.g., in central Asia and southern Africa, where a negative trend in the SAT usually corresponded with a positive trend in precipitation in most of the reanalyses (not shown).

Precipitation linearly decreased in MAM in most BRm zones, except for the EC region (Fig. 6c). The decreased precipitation over the SA and EA regions could advance aridity and increase the size of the arid regions. By contrast, the decrease in precipitation in the SW and EW regions did not increase the local BRm.

In JJA, most reanalyses showed a decrease in precipitation over the EC, EW and SW regions. The changes in precipitation in the EA and SA regions diverged between the datasets. Decreased precipitation and enhanced evaporation due to surface warming (Fig. 5d) in the EC regions could result in a reduction in ice cover over Greenland (Luthcke et al., 2006).

Precipitation in SON increased in the SA and EC regions, but decreased in the EW regions. The increase in precipitation did not slow down the rate of warming in EC regions, and the trend for averaged SAT in EC regions was the largest of all the BRm zones.

The characteristics of surface climate change over differ-

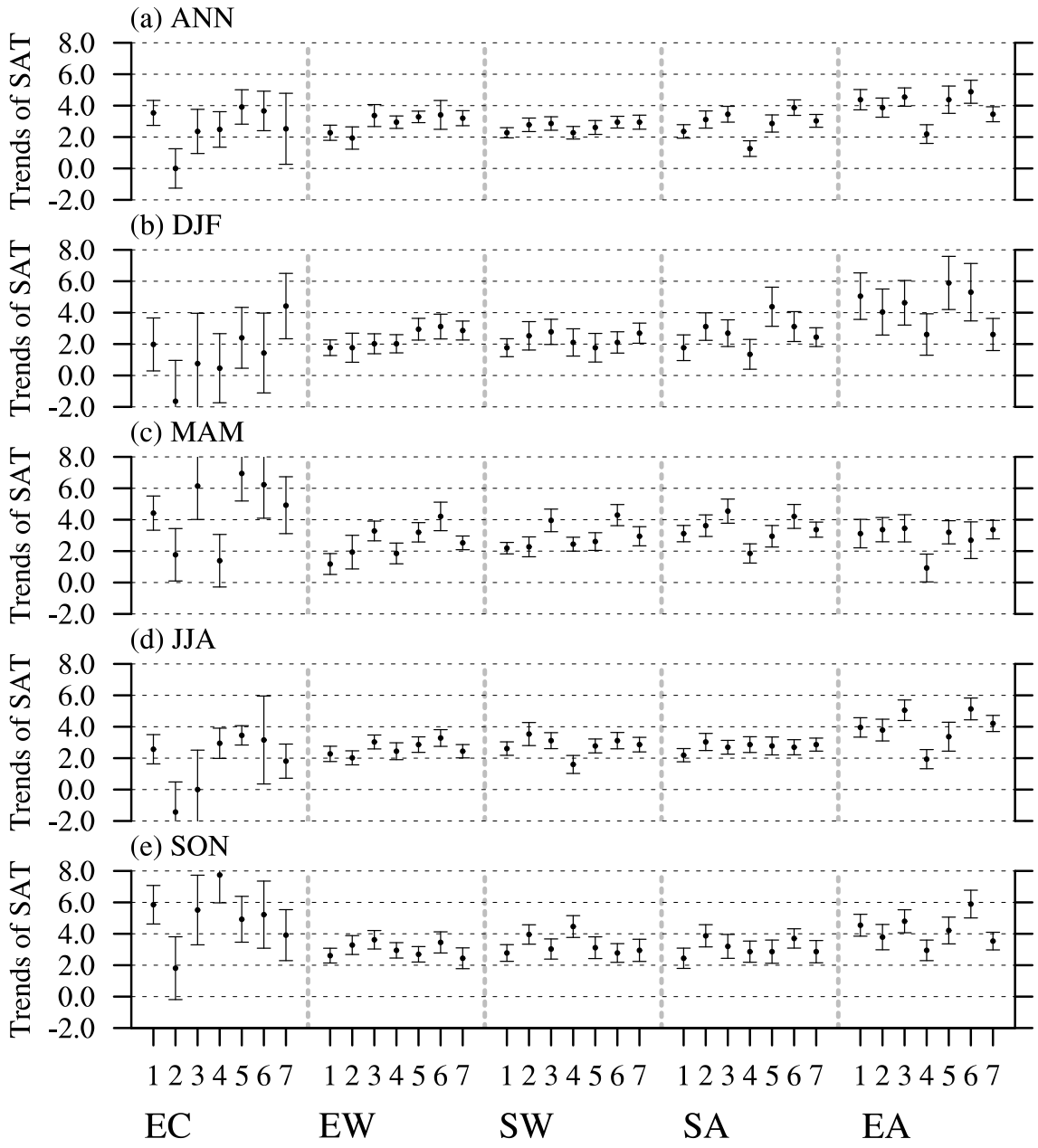

Fig. 5. Linear trends in the surface air temperature (SAT; units: 10^{-2} K yr^{-1}) for different BR zones during the time period 1980–2010. The number on the abscissa represents different datasets: 1, ensemble mean of the reanalysis data; 2, 20thC; 3, ERA-I; 4, NCEP-R1; 5, NCEP-R2; 6, JRA55; and 7, GLDAS dataset.

ent land surfaces can be discussed based on the BRm. However, links among the change of SAT, precipitation and BR are quite complicated, depending on the locations and factors, like the vegetation cover, precipitation type, etc. So, it is difficult to directly attribute the change of BRm to SAT and precipitation without any assumption. But, it is certain that changes in surface climate will cause responses in land–air interactions.

3.4. *Changes in the Bowen ratio zones*

In addition to giving a subjective climate classification map, the BRm can be calculated over any time interval from daily to yearly. This makes it suitable for discussing temporal variations in climatic zones based on the surface heat flux. The linear trends derived for the annual coverage of BRm zones in each season were investigated. The differences among the datasets need to be taken into account, but the datasets contain common features. The trend in change in area for each BRm zone was of the order of 10^{10} m^2 yr^{-1}. At this rate, the area of the BRm zones will change by less than 10% on a centennial timescale.

Using the annual means, an increase in size of the EA regions and a decrease in the size of the SA regions were suggested by five of the datasets and the EM (Fig. 7), but not by the NCEP-R1 and GLDAS datasets. This corresponds to an aridification process in these two BRm zones. An aridifica-

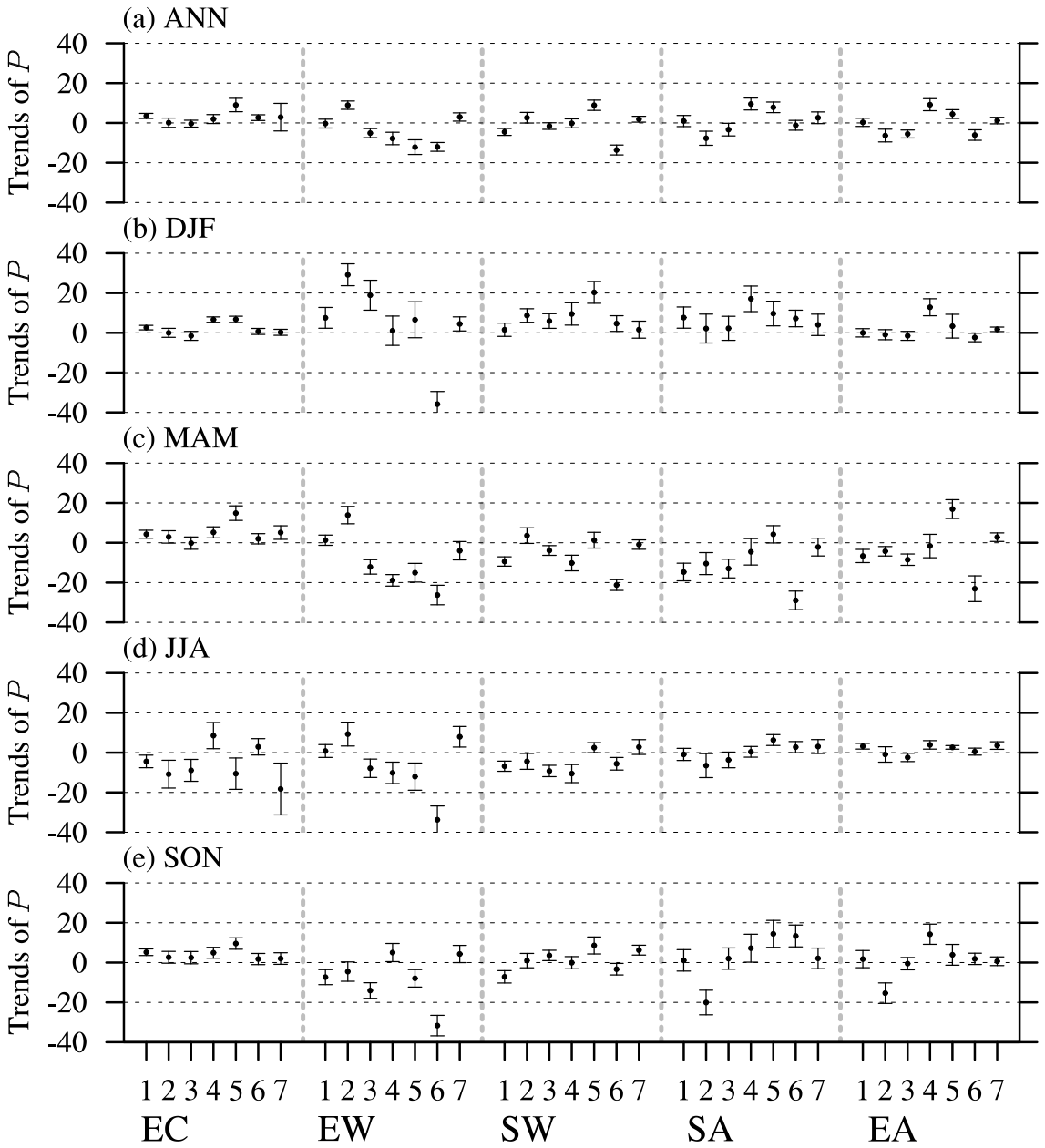

Fig. 6. Linear trends in the precipitation rate (units: 10^{-6} kg s^{-1} m^{-2} yr^{-1}) for different BR zones during the time period 1980–2010. The number on the abscissa represents different datasets: 1, ensemble mean of the reanalysis data; 2, 20thC; 3, ERA-I; 4, NCEP-R1; 5, NCEP-R2; 6, JRA55; and 7, GLDAS dataset. For convenience of display, the results for SA and EA (both trend and error) are multiplied by 2 and 4, respectively.

tion process over a similar time period has been reported previously (Nicholson, 2001; Ma and Fu, 2007; Dai, 2011). The aridification process was associated with prominent surface warming in the EA and SA regions (Fig. 5a). The reduction in precipitation in these two BRm zones, seen in three of the six datasets, is also a likely cause of aridification (Fig. 6a).

In DJF, an increase in the size of the EW regions and a decrease in the size of the SW regions were suggested by most of the datasets. An increase in precipitation was probably responsible for these changes (Fig. 6b). In the mid- to high-latitude areas of the Northern Hemisphere, the EC regions expanded at the expense of the EW regions. The increase in winter precipitation in the formerly EW regions at high latitudes may enhance the snow cover and therefore produce new EC areas.

The change in the BRm in MAM is interesting because all the datasets except for NCEP-R1 showed increases in the EA and EW regions and a decrease in the SA and SW regions in the time period 1980–2010. In other words, the SA regions were becoming EA regions and the SW regions were becoming EW regions on a global scale. A decrease in precipitation in the SA and EA regions was seen in four reanalyses (Fig.

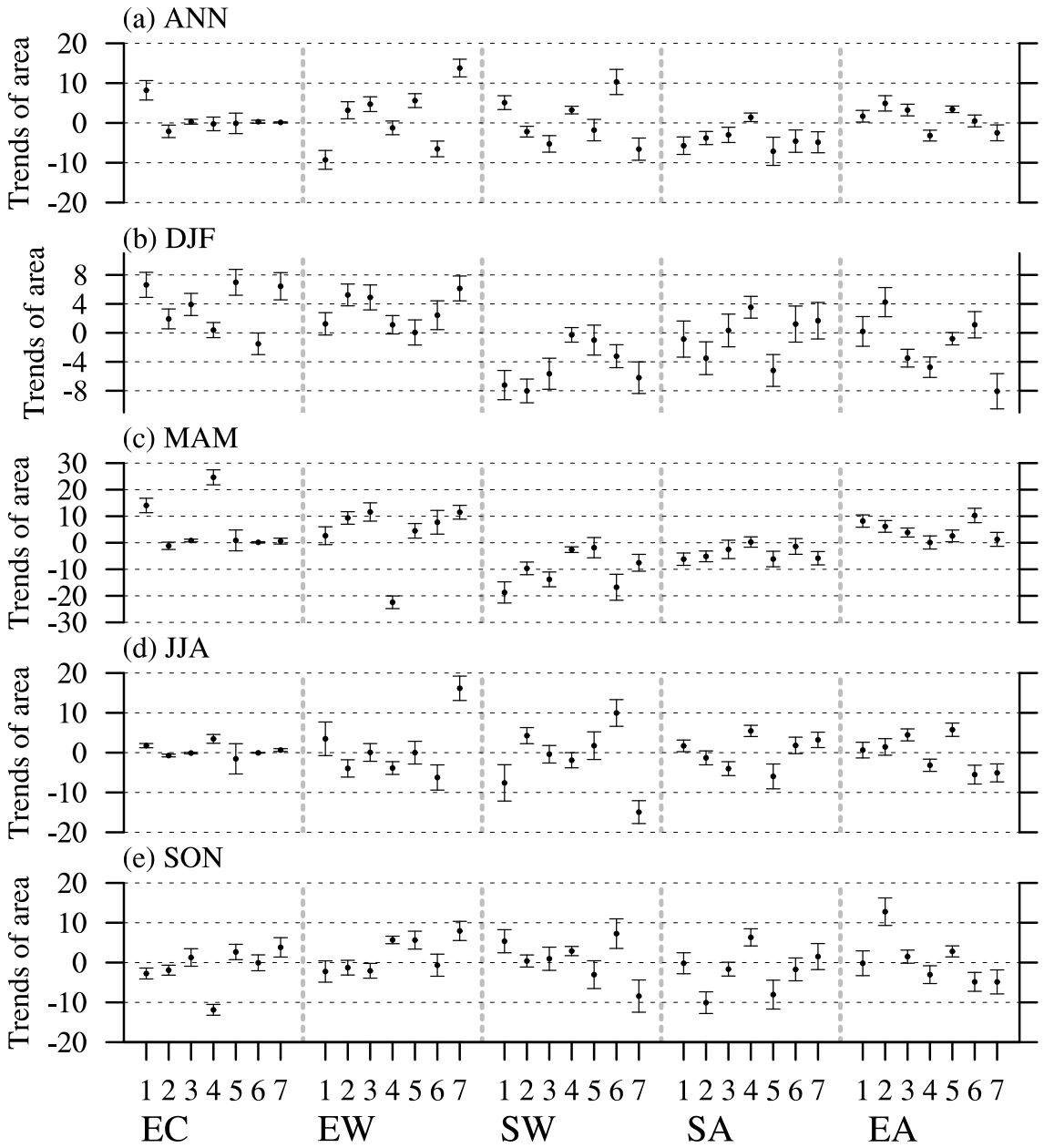

Fig. 7. Linear trends of coverage area for each BR zone (units: 10^{10} m^2 yr^{-1}) during the period 1980–2010. The number on the abscissa represents different datasets: 1, ensemble mean of the reanalysis data; 2, 20thC; 3, ERA-I; 4, NCEP-R1; 5, NCEP-R2; 6, JRA55; and 7, GLDAS dataset.

6c), which was probably responsible for the change in the size of the regions. A decrease in precipitation over the EW and SW regions was also seen in five datasets. It is expected that the BRm in the SA and EA regions will be more sensitive to local changes in precipitation than that in the SW and EW regions in MAM.

The drying process in arid regions and the moistening process in wet regions were more obvious in certain regions (Fig. 8). The greatest increase in the BRm was in Northeast Africa and the Arabian Peninsula in all seasons, with a trend in the BRm of about 1 yr^{-1}. The increase in BRm was also seen over the southwest coast of North America, central Australia and eastern Brazil, but the increase was lower. By contrast, the two main tropical forest regions, the Congo and Amazon River basins, both showed a decrease in BRm. The changes in BRm suggested that the arid regions became drier and the wet regions became moister over the period 1980–2010. However, there were also some exceptions, including a significantly decreased BRm over some SA and EA regions, e.g. northwestern and southern Africa and northwestern China.

4. Summary

This study analyzed global land surface characteristics from the viewpoint of BRs using five reanalyses and an offline

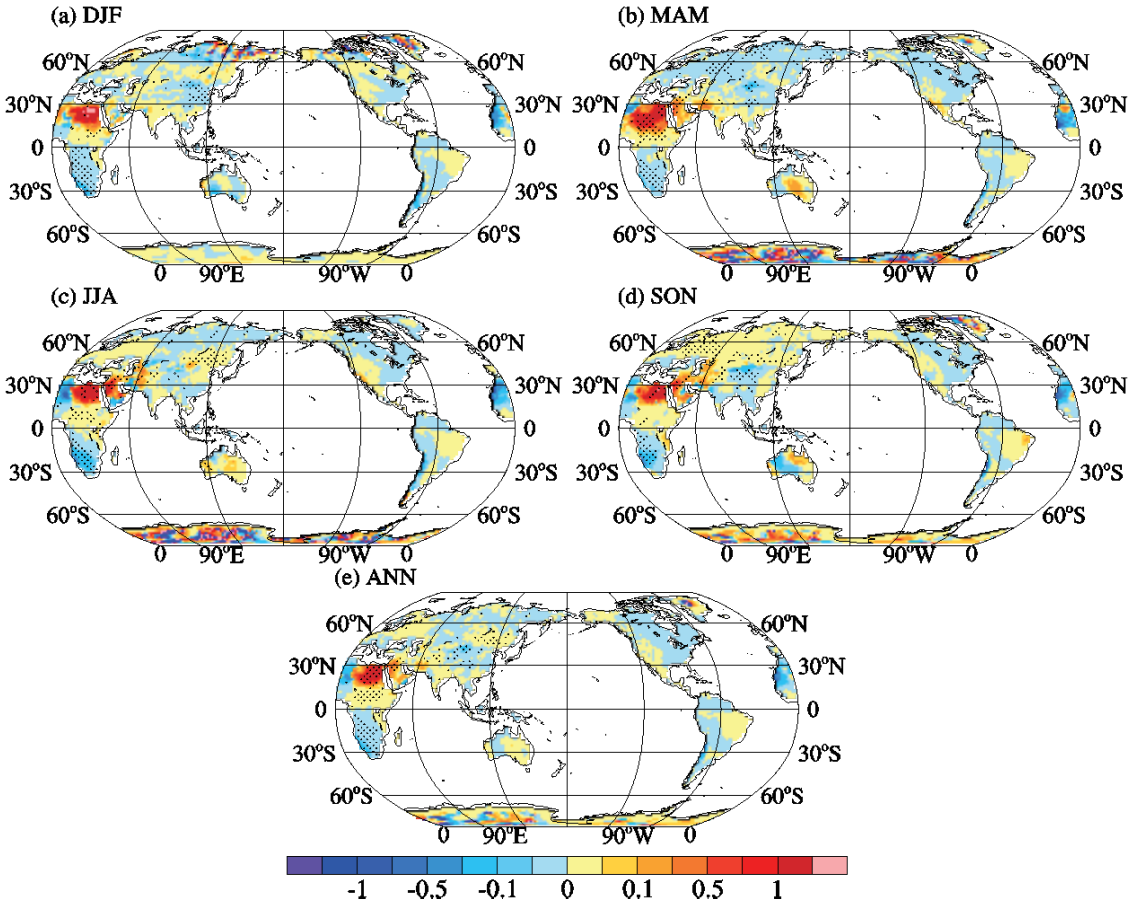

Fig. 8. Linear trends in BRm (units: yr^{-1}) during the period 1980–2010 for different seasons (a–d) and the annual means (e). All trends are derived from the EM of five reanalyses. The dotted area indicates the significance of the trend based on the EM ($P < 0.05$) and at least three reanalyses that produced the same sign for the trend.

land surface model. When the sign of the BR was determined by the direction of the surface sensible heat flux, the modified BR [i.e., BRm, Eq. (2)] captured the major divisions of the global continental climate classification with reference to the KCC. Five major divisions were identified: EC, EW, SW, SA and EA. Their corresponding BRm ranges were ($-\infty$ to 0), (0–0.5), (0.5–2), (2–10) and (10 to $+\infty$). Subdivisions were obtained by comparing the seasonal variation in the types of BRm.

We used the BRm method to investigate climate change over different kinds of land surface. The EC regions showed the largest rate of warming in MAM and SON, whereas the EA regions had the fastest warming rates in DJF and JJA, and with respect to the annual mean value. Changes in precipitation showed large differences among the different reanalysis datasets. All the BRm zones except for the EC region showed decreased precipitation in MAM.

In addition to giving a climate classification map similar to the KCC, the BRm can also describe the change in area over time for each BRm zone. The results from most datasets showed that the areas of the EA and EW regions increased over the period 1980–2010, whereas those of the SA and SW regions decreased in MAM. Thus, based on the BRm, wet regions are becoming even wetter and arid regions are becoming even drier in MAM. Because the decrease in precipitation in global EW, SW, SA and EA regions was seen in at least four of the six datasets, the changes in areas suggest that the BRm in the SA and EA regions is more sensitive to changes in precipitation than that in the EW and SW regions in MAM.

Although a global observation network for land surface fluxes has not yet been established, an increasing amount of data from climate models is being published and is free to use in scientific studies. Surface heat fluxes are often available in these products, and thus global BRm zones can be obtained in a comparable manner to the climate classification investigated in this study. In addition to giving a climatological mean distribution, the change in coverage of BRm zones reflects changes in climatic regimes. However, there are still considerable uncertainties in land surface models and, therefore, for the surface heat fluxes produced by them (like reanalyses and GLADS). The climatological mean of globally averaged BRm values in different datasets have large discrepancies (Fig. 2), as does the precipitation in each BR zone (Fig. 4). These differences can be even greater for certain regions or periods, which might limit the usefulness of the BR in representing climate zones. Nevertheless, by verify-

ing the threshold values corresponding to the five BR zones, and with reference to the KCC, the BRm can still be useful in climate classification.

Acknowledgements. We are extremely grateful to the two anonymous reviewers for their constructive suggestions and comments. This research was jointly funded by the Research Project for Public Welfare Industry (Meteorology) from the Ministry of Science and Technology in China (Grant No. GYHY201506001), the National Natural Science Foundation of China (Grant Nos. 91537214, 41675015, 41405079 and 41405020), and the Opening Research Foundation of the Key Laboratory of Land Surface Process and Climate Change in Cold and Arid Regions (Grant No. LPCC201504).

REFERENCES

Aselmann, I., and P. J. Crutzen, 1989: Global distribution of natural freshwater wetlands and rice paddies, their net primary productivity, seasonality and possible methane emissions. *Journal of Atmospheric Chemistry*, **8**(4), 307–358.

Baldocchi, D. D., 2003: Assessing the eddy covariance technique for evaluating carbon dioxide exchange rates of ecosystems: Past, present and future. *Global Change Biology*, **9**(4), 479–492, doi: 10.1046/j.1365-2486.2003.00629.x.

Baldocchi, D., R. Valentini, S. Running, W. Oechel, and R. Dahlman, 1996: Strategies for measuring and modelling carbon dioxide and water vapour fluxes over terrestrial ecosystems. *Global Change Biology*, **2**(3), 159–168, doi: 10.1111/j.1365-2486.1996.tb00069.x.

Baldocchi, D., and Coauthors, 2001: FLUXNET: A new tool to study the temporal and spatial variability of ecosystem-scale carbon dioxide, water vapor, and energy flux densities. *Bull. Amer. Meteor. Soc.*, **82**(11), 2415–2434, doi: 10.1175/1520-0477(2001)082<2415:Fantts>2.3.Co;2.

Bintanja, R., 2000: Surface heat budget of Antarctic snow and blue ice: Interpretation of spatial and temporal variability. *J. Geophys. Res.*, **105**(D19), 24 387–24 407, doi: 10.1029/2000jd900356.

Bounoua, L., G. J. Collatz, S. O. Los, P. J. Sellers, D. A. Dazlich, C. J. Tucker, and D. A. Randall, 2000: Sensitivity of climate to changes in NDVI. *J. Climate*, **13**(13), 2277–2292, doi: 10.1175/1520-0442(2000)013<2277:Soctci>2.0.Co;2.

Bowen, I. S., 1926: The ratio of heat losses by conduction and by evaporation from any water surface. *Phys. Rev.*, **27**(6), 779–787, doi: 10.1103/PhysRev.27.779.

Bradley, R. S., H. F. Diaz, G. N. Kiladis, and J. K. Eischeid, 1987: Enso signal in continental temperature and precipitation records. *Nature*, **327**(6122), 497–501, doi: 10.1038/327497a0.

Budyko, M. I., 1961: The heat balance of the earth's surface. *Soviet Geography*, **2**(4), 3–13.

Chen, M. Y., P. P. Xie, J. E. Janowiak, and P. A. Arkin, 2002: Global land precipitation: A 50-yr monthly analysis based on gauge observations. *Journal of Hydrometeorology*, **3**(3), 249–266, doi: 10.1175/1525-7541(2002)003<0249:Glpaym>2.0.Co;2.

Compo, G. P., and Coauthors, 2011: The twentieth century reanalysis project. *Quart. J. Roy. Meteor. Soc.*, **137**(654), 1–28, doi: 10.1002/Qj.776.

Condit, R., S. P. Hubbell, and R. B. Foster, 1996: Assessing the response of plant functional types to climatic change in tropical forests. *Journal of Vegetation Science*, **7**(3), 405–416, doi: 10.2307/3236284.

Dabberdt, W. F., D. H. Lenschow, T. W. Horst, P. R. Zimmerman, S. P. Oncley, and A. C. Delany, 1993: Atmosphere-surface exchange measurements. *Science*, **260**(5113), 1472–1481, doi: 10.1126/science.260.5113.1472.

Dai, A. G., 2011: Drought under global warming: A review. *Wires Climate Change*, **2**(1), 45–65, doi: 10.1002/wcc.81.

Dai, A. G., and T. M. L. Wigley, 2000: Global patterns of ENSO-induced precipitation. *Geophys. Res. Lett.*, **27**(9), 1283–1286, doi: 10.1029/1999gl011140.

Dee, D. P., and Coauthors, 2011: The ERA-Interim reanalysis: Configuration and performance of the data assimilation system. *Quart. J. Roy. Meteor. Soc.*, **137**(656), 553–597, doi: 10.1002/Qj.828.

Defries, R. S., and J. R. G. Townshend, 1994: Ndvi-derived land cover classifications at a global scale. *Int. J. Remote Sens.*, **15**(17), 3567–3586.

den Hartog, G., H. H. Neumann, K. M. King, and A. C. Chipanshi, 1994: Energy budget measurements using eddy correlation and Bowen ratio techniques at the Kinosheo lake tower site during the northern wetlands study. *J. Geophys. Res.*, **99**(D1), 1539–1549, doi: 10.1029/93jd00032.

Ek, M. B., K. E. Mitchell, Y. Lin, E. Rogers, P. Grunmann, V. Koren, G. Gayno, and J. D. Tarpley, 2003: Implementation of Noah land surface model advances in the National Centers for Environmental Prediction operational mesoscale Eta model. *J. Geophys. Res.*, **108**(D22), doi: 10.1029/2002JD003296.

Elguindi, N., A. Grundstein, S. Bernardes, U. Turuncoglu, and J. Feddema, 2014: Assessment of CMIP5 global model simulations and climate change projections for the 21st century using a modified Thornthwaite climate classification. *Climatic Change*, **122**(4), 523–538, doi: 10.1007/s10584-013-1020-0.

Feng, S., C.-H. Ho, Q. Hu, R. J. Oglesby, S.-J. Jeong, and B.-M. Kim, 2012: Evaluating observed and projected future climate changes for the Arctic using the Köppen-Trewartha climate classification. *Climate Dyn.*, **38**(7–8), 1359–1373, doi: 10.1007/s00382-011-1020-6.

Fensholt, R., and Coauthors, 2012: Greenness in semi-arid areas across the globe 1981–2007—An Earth Observing Satellite based analysis of trends and drivers. *Remote Sensing of Environment*, **121**, 144–158, doi: 10.1016/j.rse.2012.01.017.

Fisher, J. B., K. P. Tu, and D. D. Baldocchi, 2008: Global estimates of the land-atmosphere water flux based on monthly AVHRR and ISLSCP-II data, validated at 16 FLUXNET sites. *Remote Sensing of Environment*, **112**(3), 901–919, doi: 10.1016/j.rse.2007.06.025.

Gallardo, C., V. Gil, E. Hagel, C. Tejeda, and M. de Castro, 2013: Assessment of climate change in Europe from an ensemble of regional climate models by the use of Köppen-Trewartha classification. *International Journal of Climatology*, **33**(9), 2157–2166, doi: 10.1002/joc.3580.

Gan, M. A., V. E. Kousky, and C. F. Ropelewski, 2004: The South America monsoon circulation and its relationship to rainfall over west-central Brazil. *J. Climate*, **17**(1), 47–66, doi: 10.1175/1520-0442(2004)017<0047:Tsamca>2.0.Co;2.

Giorgi, F., and Coauthors, 2001: Emerging patterns of simulated regional climatic changes for the 21st century due to anthropogenic forcings. *Geophys. Res. Lett.*, **28**(17), 3317–3320, doi: 10.1029/2001gl013150.

Golluscio, R. A., and O. E. Sala, 1993: Plant functional types and

ecological strategies in Patagonian forbs. *Journal of Vegetation Science*, **4**(6), 839–846, doi: 10.2307/3235623.

Holmgren, M., and Coauthors, 2006: Extreme climatic events shape arid and semiarid ecosystems. *Frontiers in Ecology and the Environment*, **4**(2), 87–95, doi: 10.1890/1540-9295(2006)004[0087: Ecesaa]2.0.Co;2.

Huang, J., X. Guan, and F. Ji, 2012: Enhanced cold-season warming in semi-arid regions. *Atmospheric Chemistry and Physics*, **12**(12), 5391–5398, doi: 10.5194/acp-12-5391-2012.

Huete, A. R., and Coauthors, 2006: Amazon rainforests green-up with sunlight in dry season. *Geophys. Res. Lett.*, **33**(6), L06405, doi: 10.1029/2005gl025583.

Inman-Bamber, N. G., and M. G. McGlinchey, 2003: Crop coefficients and water-use estimates for sugarcane based on long-term Bowen ratio energy balance measurements. *Field Crops Research*, **83**(2), 125–138, doi: 10.1016/S0378-4290(03) 00069-8.

Jacobs, A. F. G., B. G. Heusinkveld, and S. M. Berkowicz, 2008: Passive dew collection in a grassland area, The Netherlands. *Atmospheric Research*, **87**(3–4), 377–385, doi: 10.1016/j.atmosres.2007.06.007.

Jones, P. D., M. New, D. E. Parker, S. Martin, and I. G. Rigor, 1999: Surface air temperature and its changes over the past 150 years. *Rev. Geophys.*, **37**(2), 173–199, doi: 10.1029/1999rg900002.

Kalnay, E., and Coauthors, 1996: The NCEP/NCAR 40-year reanalysis project. *Bull. Amer. Meteor. Soc.*, **77**(3), 437–471, doi: 10.1175/1520-0477(1996)077<0437:Tnyrp>2.0.Co;2.

Kanamitsu, M., W. Ebisuzaki, J. Woollen, S.-K. Yang, J. J. Hnilo, M. Fiorino, and G. L. Potter, 2002: NCEP-DOE AMIP-II reanalysis (R-2). *Bull. Amer. Meteor. Soc.*, **83**(11), 1631–1643, doi: 10.1175/Bams-83-11-1631.

Kobayashi, S., and Coauthors, 2015: The JRA-55 reanalysis: General specifications and basic characteristics. *J. Meteor. Soc. Japan*, **93**(1), 5–48, doi: 10.2151/jmsj.2015-001.

Koöppen, W. P., 1931: *Grundriss der Klimakunde*. Walter de Gruyter, Berlin.

Kottek, M., J. Grieser, C. Beck, B. Rudolf, and F. Rubel, 2006: World map of the Köppen-Geiger climate classification updated. *Meteor. Z.*, **15**(3), 259–263, doi: 10.1127/0941-2948/2006/0130.

Krishnan, P., T. P. Meyers, R. L. Scott, L. Kennedy, and M. Heuer, 2012: Energy exchange and evapotranspiration over two temperate semi-arid grasslands in North America. *Agricultural and Forest Meteorology*, **153**, 31–44, doi: 10.1016/j.agrformet.2011.09.017.

Lewis, J. M., 1995: The story behind the Bowen ratio. *Bull. Amer. Meteor. Soc.*, **76**(12), 2433–2443, doi: 10.1175/1520-0477(1995)076<2433:Tsbtbr>2.0.Co;2.

Luthcke, S. B., and Coauthors, 2006: Recent Greenland ice mass loss by drainage system from satellite gravity observations. *Science*, **314**(5803), 1286–1289, doi: 10.1126/science.1130776.

Ma, Z. G., and C. B. Fu, 2007: Global aridification in the second half of the 20th century and its relationship to large-scale climate background. *Science in China Series D: Earth Sciences*, **50**(5), 776–788, doi: 10.1007/s11430-007-0036-6.

Menon, S., J. Soberón, X. G. Li, and A. T. Peterson, 2010: Preliminary global assessment of terrestrial biodiversity consequences of sea-level rise mediated by climate change. *Biodiversity and Conservation*, **19**(6), 1599–1609, doi: 10.1007/s10531-010-9790-4.

Middleton, N., and D. Thomas, 1997: *World Atlas of Desertification*. 2nd ed. Arnold, London.

Navarro, T., C. L. Alados, and B. Cabezudo, 2006: Changes in plant functional types in response to goat and sheep grazing in two semi-arid shrublands of SE Spain. *Journal of Arid Environments*, **64**(2), 298–322, doi: 10.1016/j.jaridenv.2005.05.005.

Nicholson, S. E., 2001: Climatic and environmental change in Africa during the last two centuries. *Climate Research*, **17**(2), 123–144, doi: 10.3354/cr017123.

Nicolas, J. P., and D. H. Bromwich, 2014: New reconstruction of Antarctic near-surface temperatures: Multidecadal trends and reliability of global reanalyses. *J. Climate*, **27**, 8070–8093.

Olson, D. M., and Coauthors, 2001: Terrestrial ecoregions of the world: A new map of life on Earth. *BioScience*, **51**(11), 933–938, doi: 10.1641/0006-3568(2001)051[0933:Teotwa]2.0.Co;2.

Paltineanu, C., E. Chitu, and E. Mateescu, 2011: Changes in crop evapotranspiration and irrigation water requirements. *International Agrophysics*, **25**(4), 369–373.

Pan, H.-L., and L. Mahrt, 1987: Interaction between soil hydrology and boundary-layer development. *Bound.-Layer Meteor.*, **38**, 185–202.

Pearch, M. J., 2011: A review of the biological diversity and distribution of small mammal taxa in the terrestrial ecoregions and protected areas of Nepal. *Zootaxa*, **3072**, 1–286.

Peel, M. C., B. L. Finlayson, and T. A. McMahon, 2007: Updated world map of the Köppen-Geiger climate classification. *Hydrology and Earth System Sciences*, **11**(5), 1633–1644.

Pitacco, A., N. Gallinaro, and C. Giulivo, 1992: Evaluation of actual evapotranspiration of a *Quercus ilex* L. stand by the Bowen ratio-energy budget method. *Vegetation*, **99**, 163–168.

Poulter, B., and Coauthors, 2014: Contribution of semi-arid ecosystems to interannual variability of the global carbon cycle. *Nature*, **509**(7502), 600–603, doi: 10.1038/Nature13376.

Ragab, R., and C. Prudhomme, 2002: SW-Soil and Water: Climate change and water resources management in arid and semi-arid regions: Prospective and challenges for the 21st century. *Biosystems Engineering*, **81**(1), 3–34, doi: 10.1006/bioe.2001.0013.

Rodell, M., and Coauthors, 2004: The global land data assimilation system. *Bull. Amer. Meteor. Soc.*, **85**, 381–394.

Rusch, G. M., J. G. Pausas, and J. Lepš, 2003: Plant Functional Types in relation to disturbance and land use: Introduction. *Journal of Vegetation Science*, **14**(3), 307–310, doi: 10.1111/j.1654-1103.2003.tb02156.x.

Sellers, P. J., Y. Mintz, Y. C. Sud, and A. Dalcher, 1986: A simple biosphere model (SiB) for use within general circulation models. *J. Atmos. Sci.*, **43**, 505–531.

Small, E. E., F. Giorgi, and L. C. Sloan, 1999: Regional climate model simulation of precipitation in central Asia: Mean and interannual variability. *J. Geophys. Res.*, **104**(D6), 6563–6582, doi: 10.1029/98jd02501.

Smith, T. M., H. H. Shugart, F. I. Woodward, and P. J. Burton, 1993: Plant functional types. *Vegetation Dynamics & Global Change*, S. M. Solomon and H. H. Shugart, Eds., Chapman & Hall, New York, 272–292.

Sun, W. Y., X. Y. Song, X. M. Mu, P. Gao, F. Wang, and G. J. Zhao, 2015: Spatiotemporal vegetation cover variations associated with climate change and ecological restoration in the Loess Plateau. *Agricultural and Forest Meteorology*, **209–210**, 87–99, doi: 10.1016/j.agrformet.2015.05.002.

Tang, L., and F. Hossain, 2012: Investigating the similarity of satellite rainfall error metrics as a function of Köppen climate classification. *Atmospheric Research*, **104–105**, 182–192, doi: 10.1016/j.atmosres.2011.10.006.

Taylor, K. E., R. J. Stouffer, and G. A. Meehl, 2012: An overview of CMIP5 and the experiment design. *Bull. Amer. Meteor. Soc.*, **93**(4), 485–498, doi: 10.1175/Bams-D-11-00094.1.

Toda, M., K. Nishida, N. Ohte, M. Tani, and K. Musiake, 2002: Observations of energy fluxes and evapotranspiration over terrestrial complex land covers in the tropical monsoon environment. *J. Meteor. Soc. Japan*, **80**(3), 465–484, doi: 10.2151/Jmsj.80.465.

Todd, R. W., S. R. Evett, and T. A. Howell, 2000: The Bowen ratio-energy balance method for estimating latent heat flux of irrigated alfalfa evaluated in a semi-arid, advective environment. *Agricultural and Forest Meteorology*, **103**(4), 335–348, doi: 10.1016/S0168-1923(00)00139-8.

Trewartha, G., and L. Horn, 1980: Köppen's classification of climates. *An Introduction to Climate*, McGraw-Hill, New York, 397–403.

Trewartha, G. T., and R. D. Sale, 1968: *An Introduction to Climate*. McGraw-Hill, New York.

Turner, J., and Coauthors, 2005: Antarctic climate change during the last 50 years. *International Journal of Climatology*, **25**(3), 279–294, doi: 10.1002/joc.1130.

Ustin, S. L., and J. A. Gamon, 2010: Remote sensing of plant functional types. *New Phytologist*, **186**(4), 795–816, doi: 10.1111/j.1469-8137.2010.03284.x.

Viterbo, P., and A. C. M. Beljaars, 1995: An improved land surface parameterization scheme in the ECMWF model and its validation. *J. Climate*, **8**, 2716–2748.

Walker, D. A., and Coauthors, 2003: Phytomass, LAI, and NDVI in northern Alaska: Relationships to summer warmth, soil pH, plant functional types, and extrapolation to the circumpolar Arctic. *J. Geophys. Res.*, **108**(D2), 8169, doi: 10.1029/2001jd000986.

Wallace, J. M., Q. Fu, B. V. Smoliak, P. Lin, and C. M. Johanson, 2012: Simulated versus observed patterns of warming over the extratropical Northern Hemisphere continents during the cold season. *Proceedings of the National Academy of Sciences of the United States of America*, **109**(36), 14 337–14 342, doi: 10.1073/pnas.1204875109.

Wang, C.-Y., C.-F. Luo, S.-H. Qi, and Z. Niu, 2005: A method of land cover classification for China based on NDVI-Ts space. *Journal of Remote Sensing*, **9**, 93–99. (in Chinese with English abstract)

Warry, N. D., and M. Hanau, 1993: The use of terrestrial ecoregions as a regional-scale screen for selecting representative reference sites for water quality monitoring. *Environmental Management*, **17**(2), 267–276, doi: 10.1007/Bf02394696.

Wilson, K., and Coauthors, 2002: Energy balance closure at FLUXNET sites. *Agricultural and Forest Meteorology*, **113**(1–4), 223–243, doi: 10.1016/S0168-1923(02)00109-0.

Woodward, F. I., and W. Cramer, 1996: Plant functional types and climatic change: Introduction. *Journal of Vegetation Science*, **7**(3), 306–308.

Yu, L. S., X. Z. Jin, and R. A. Weller, 2008: Multidecade global flux datasets from the objectively analyzed air-sea fluxes (OAFlux) project: Latent and sensible heat fluxes, ocean evaporation, and related surface meteorological variables. OAFlux Project Technical Report (OA-2008-01), Woods Hole Oceanographic Institution.

Zhang, Q. F., G. X. Liu, and Y. H. Bao, 2014: Review of drought monitoring indicators. *Sixth Annual Meeting of Information Technology for Risk Analysis and Crisis Response Committee*, 23 August 2014, Inner Mongolia, China, 117–122. (in Chinese)

Zhou, J. Y., and K. M. Lau, 1998: Does a monsoon climate exist over South America. *J. Climate*, **11**(5), 1020–1040, doi: 10.1175/1520-0442(1998)011<1020:Damceo>2.0.Co;2.

Zhou, L., R. K. Kaufmann, Y. Tian, R. B. Myneni, and C. J. Tucker, 2003: Relation between interannual variations in satellite measures of northern forest greenness and climate between 1982 and 1999. *J. Geophys. Res.*, **108**(D1), ACL 3-1–ACL 3-16, doi: 10.1029/2002jd002510.